Journal of Applied Mechanics and Technical Physics

(Siberian Branch of the Russian Academy of Sciences)

ISSN: 0021-8944 (Print) 1573-8620 (Online); Publisher: Springer; Impact Factor = 0.643

Accepted June 17th 2019

Entropy Analysis on Convective Film Flow of Power-law Fluid with Nanoparticles along an Inclined Plate

B. Vasu[1*], Rama Subba Reddy Gorla[2], P. V. S. N. Murthy[3] *and* **O. Anwar Bég[4]**

[1]*Department of Mathematics, Motilal Nehru National Institute of Technology Allahabad, Prayagraj -211004,* ***India***
[2]*Department of Mechanical Engineering, Cleveland State University, Ohio, 44115,* ***USA***
[3]*Department of Mathematics, Indian Institute of Technology Kharagpur, Kharagpur, India.*
[4]*Department of Mechanical and Aeronautical Engineering, Salford University, Salford, M54WT,* ***UK****.*
****Corresponding author- Email:*** *bvasu@mnnit.ac.in*

ABSTRACT

Entropy generation in two-dimensional, steady, laminar thin film convection flow of a non-Newtonian nanofluid (Ostwald-de Waele type power law fluid with embedded nanoparticles) along an inclined plate is examined theoretically. A revised Buongiorno model is adopted for nanoscale phenomena which includes the effects of Brownian motion and thermophoresis and for which the nanofluid particle fraction on the boundary is *passively* rather than *actively* controlled. A convective boundary condition is employed. The local non-similarity method is used to solve the non-dimensional, non-linear emerging system of governing equations. Validation with earlier published results is included. A decrease in the entropy generation is induced due to fluid friction associated with increasing value of the rheological power law index (n). Brownian motion (Nb) of nanoparticles enhances thermal convection via the enhanced transport of heat in micro-convection surrounding individual nanoparticles. Higher convective parameter ($\boldsymbol{\gamma}$) implies stronger convective heating at the plate, which increases the temperature gradient. Increasing thermophoresis parameter decreases nano-particle volume fraction near the wall but increases it further from the wall. Entropy generation is also reduced with increasing thermophoresis effect throughout the boundary layer. The results are relevant to thermodynamic optimization of non-Newtonian thin film flows in coating materials processing operations.

KEYWORDS: *Entropy Analysis, Film Flow, Nanofluid, Free Convection, Power-law Model, Brownian motion, Thermophoresis.*

1. Introduction

The analysis of the flow of an incompressible liquid film over an inclined surface has important applications in many branches of science and engineering including polymer processing

(extrusion), film coating and surface treatment. Other applications include wire and fiber coating, food stuff processing, reactor fluidization, transpiration cooling, anti-corrosion protection etc. An understanding of flow and heat transfer within a thin film in the coating process is crucial. In manufacturing processes, the melt issues from a slit and is subsequently stretched to achieve the desired thickness. The constitution and homogeneity of the final product is strongly dependent on the interaction of mechanical forces and thermal conditions and is therefore highly dependent on the nature of the hydrodynamics and heat transfer characteristics in the vicinity of the sheet. Robust mathematical models and computational simulations of the film fluid dynamics and heat transport intrinsic to such processes provide an excellent and inexpensive mechanism for improving material design and performance. The rheological properties of thin film made by tape casting have attracted the attention of many researchers. Wang [1] derived analytical solutions for flow of a Newtonian liquid film on an unsteady stretching surface. Since numerous industrial coating liquids are rheological in nature, Anderson and Irgens [2] presented a theoretical analysis of steady laminar film flow of power-law fluids within the framework of classical boundary layer theory. The study demonstrated that the approximate integral method solutions for flow in the upstream region closely corresponds to the similarity solution of the flow. Gorla and Nee [3] analysed the entrance region heat transfer to a laminar, non-Newtonian falling liquid film with a fully developed velocity profile using a perturbation method. Shang and Anderson [4] presented a model for falling liquid film flow of power-law fluid with heat transfer. Gorla *et al.* [5] studied the entropy analysis in the micro/nano scale thin film flow in a capillary tube.

Enhancement of heat transfer in engineering applications is very important because conventional fluid such as oil, water that are used in various technologies possess relatively low thermal conductivity. The thermal performance of such conventional base fluids can be upgraded by dispersion of nano-sized particle. The resultant combination of base fluid and nano-sized particles (nanoparticles) is known as a *nanofluid*. Nanofluids are therefore engineered colloids which have been shown to exhibit high, non-linear and anomalous thermal conductivity, compared to the base fluid and to achieve significant elevations in heat transfer rates. Nanofluid dynamics involves four scales: the *molecular scale, the microscale, the macroscale* and *the mega-scale* and an interaction is known to take place between these scales. Diverse types of nanofluids can be synthesized by combining different nano-particles (e.g. metallic oxides, silicon carbides, carbon nanotubes) with different base fluids. Nanofluids were introduced by Choi [6] in the 1990s and have been applied in a diverse range of engineering systems including medical, energy and materials sciences. An important area of interest has been nano-coatings [7] in which thin nano-structured films are deposited on surfaces which require protection from corrosion, abrasion, degradation, acidic attack

etc. Phan *et al.* [8] have deployed nanofluid coatings to improve surface wettability in phase-change heat transfer. Bég *et al.* [8] explored the deployment of thin film nano-polymeric coatings for solar collector surfaces. Sorrentino described the advantages of thin film nano-coatings for packaging in electronics and other sectors since they offer the achieve advantage of highly thermally conductive materials which facilitate effective heat dissipation and offer enhanced protection to sensitive components. Ullah *et al.* [11] have considered unsteady flows of thin nano-film coatings for polymeric systems. Many modelling approaches have been developed to simulate the diverse characteristics of nanofluids. The most popular of these approaches has been the two-component non-homogenous Buongiorno model [12] which analyses momentum, heat and mass transfer (and includes Brownian dynamics and thermophoresis). Another approach is the Tiwari-Das model [13] which allows volume fraction and specific nano-particles to be studied but only provides a formulation for momentum and energy transfer and ignores mass transfer. This model however enables the nanofluid properties (e.g. viscosity, thermal conductivity, density and heat capacity) to be calculated at different volume fractions for any nano-particle (zinc, gold, silica, iron oxide etc). Although other formulations have been developed such as the Pak-Cho model [14], the other formulations have emerged as the most popular and are more easily accommodated in thin film thermofluid dynamics. Kuznetsov and Nield [15] were among the first to investigate the free convective flow of a nanofluid from a vertical plate with the Buongiorno model. Tripathi *et al.* [16] also employed the Buongiorno model to study electro-osmotic peristaltic pumping of aqueous ionic nanofluids with symbolic software (Mathematica). Kasmani *et al.* [17] used a Runge-Kutta-Gill numerical method and Boungiorno's model to compute laminar nanofluid convection boundary layer flow over a wedge with wall transpiration effects. They observed that Brownian motion and thermophoresis considerably modified the temperature and nano-particle volume fraction (concentration) distributions. The Tiwari-Das model has also been used extensively in nanofluid modelling. Kuharat *et al.* [18] investigated copper oxide, titanium oxide and silver oxide metallic nano-particle effects on thermal efficiency of a solar enclosure with the Tiwari-Das model, ANSYS Fluent software and multiple radiative heat transfer models, observing that optimum doping can lead to significant elevations in thermal performance. Loganthan *et al.* [19] used a Laplace transform method and the Tiwari-Das model to compute the influence of heat generation and nanoparticle volume concentration on unsteady nanofluid natural convection from an impulsively started vertical surface. They examined aluminum oxide, copper, titanium oxide, and silver nanoparticles with a volume concentration range of up to 4%, observing that the best heat transfer is achieved in silver–water nanofluid.

Choi [6] established the rheological nature of nanofluids and the influence of volume concentrations on shear behaviour. These have further been confirmed in several investigations subsequently. For example, Ahmadi *et al.* [20] verified experimentally the significant influence of nanoparticle size and shear rate on rheological behavior of nanofluids. Sharma *et al*. [21] elaborated on the substantial contribution of particle shape, concentration (volume fraction), shear rate range, and other characteristics on the non-Newtonian behaviour of any nanofluid, also noting that the rheological nature of nanofluids is more prominent at high shear rates. Chen *et al.* [22] considered ethylene glycol (EG)-based nanofluids containing 0.5–8.0 wt% spherical TiO_2 nanoparticles at 20–60 °Celsius and observed that shear thinning behaviour is a function of the effective particle concentration, the range of shear rate and viscosity of the base liquid. They further proposed that the non-Newtonian characteristic shear rate decreases with increasing volume fraction, increasing base liquid viscosity, or increasing aggregate size. They also noted that characteristic shear rate is reduced at higher temperature, and the nanofluid behaves more as a shear-thinning suspension, since Brownian diffusion dominates at a higher temperature. Many theoretical studies of non-Newtonian nanofluid flows have also been reported in recent years featuring a diverse array of rheological models. Vasu and Ray [23] studied the non-Fourier free convection heat transfer in a Carreau nanofluid with periodic variations of surface temperature and the concentration of species using a homotopy method. They observed shear thinning nanofluid is accelerated by increasing the Weissenberg number whereas it is decelerated for a shear thickening fluid. Temperatures were also computed as lower than the Fourier model and thermal boundary layer thickness was shown to be larger with an increase in thermophoresis and Brownian motion parameter. Oyelakin *et al*. [24] analysed time-dependent viscoplastic nanofluid Sakiadis flow with radiative heat transfer, slip and cross diffusion effects with a spectral relaxation method and Buongiorno's model. Gorla and Gireesha [25] investigated laminar time-independent viscoelastic nanofluid boundary layer flow from a convective stretching surface with a Runge–Kutta–Fehlberg method with the shooting technique. A much simpler model, the Ostwald-deWaele power-law model was employed in careful experimental testing by Studart *et al.* [26] and shown to be very accurate for metallic nanofluid suspensions (e.g. titanium nano-particles in distilled water, ethylene glycol-distilled water, and propylene glycol-distilled water mixtures). It was found that distilled water base fluid generally shows stronger shear-thinning behaviour than glycol-distilled water mixture particularly at low shear rate. Various researchers have adopted the power-law model in computational nanofluid simulations since it permits two distinct categories of behaviour to be studied- pseudoplastic and dilatant, (in addition to Newtonian behaviour) depending on the power-

law rheological index. It is important also to note that in nanofluid rheology modelling, it is vital to use models for the apparent viscosity which are valid over the entire range of shear rates. The colloidal interaction between nano-particles, leads to the shear flow of nanofluids indicating shear-thinning behaviour or pseudoplasticity. Pseudoplastics are purely viscous time-independent fluids without the yield stress in which their apparent viscosity decreases with increasing shear rate. To analyze the shear-thinning (or thickening) flow behavior of nanofluid, the rheological power law fluid model is the most robust approach available. Hayat *et al.* [27] presented homotopy solutions for the boundary layer flow of a power-law non-Newtonian nanofluid induced by a vertical stretching sheet. Gorla and Vasu [28] used the Buongiorno model and Keller-box implicit finite difference method to study numerically the unsteady forced convective power-law nanofluid boundary layer flow from a stretching sheet. Ferdows and Hamad [29] used the Tiwari-Das nanoscale and power-law rheological models to investigate steady-state mixed convection boundary layer flow of an electrically-conducting nanofluid (copper-water) from a stretching surface under an alternating magnetic field and buoyancy forces. Aziz *et al.* [30] investigated variable thermal conductivity effects in transient hydromagnetic power-law nanofluid slip flow. These studies all confirmed the significant variation in thermofluid characteristics in nanofluids with power-law rheology.

In numerous industrial heat transfer processes e.g. thermal nano-coating, convective surface boundary conditions arise. The heat supplied to the convective fluid through a boundary surface with a finite heat capacity mimics more realistically the transport phenomena in nano-spray deposition, thin film coating, laser pulse heating and other applications. Convective boundary conditions may feature thermal and also species Biot numbers. Makinde and Aziz [31] presented numerical solutions for the boundary layer flow from a stretching sheet in a nanofluid incorporating the effect of a convective boundary condition. They observed that temperatures and local nano-particle concentrations are enhanced with increasing thermal Biot number (intensified convective heating). Kameswaran *et al*. [12] analysed the non-Boussinesq mixed convection from a wavy surface embedded in a porous medium with both convective temperature and concentration boundary conditions. Bég *et al.* [33] used pseudo-spectral, variational iterative and Maple quadrature methods to investigate convective cooling in exothermically-reacting non-Newtonian convection in gels in cylindrical conduits (propulsion ducts), observing that thermal Biot number modifies temperature distributions significantly. Uddin *et al*. [34] studied the impact of species and thermal convective boundary conditions on power-law nanofluid flow under radiative flux in a permeable regime. They showed that both temperature and nanoparticle concentration values

are elevated with convection-diffusion effect and that the flow is decelerated with increasing greater power-law rheological index whereas temperatures are enhanced.

In thermal coating processes energy losses are incurred which can cause disorder (entropy). The mitigation or reduction of energy losses is now a major focus in manufacturing systems. Analysis of entropy generation is a powerful tool enabling the minimization of energy wastage or the optimum utilization for maximizing system performance. Bejan [35] pioneered the entropy generation minimization (EGM) approach. Since generically thermal processes are inherently irreversible, this leads to continuous entropy generation, which eliminates the exergy (useful energy or available energy for work) of a system via different modes of heat transfer (thermal conduction, convection and radiation). Numerous other phenomena may also contribute to the entropy production including electrical fields, magnetic fields, viscosity (fluid friction), magnetic field, thermal buoyancy, species buoyancy etc. Minimization in the loss of exergy in any system is desirable since it permits optimal usage of the energy situation with minimum irreversibilities. This optimum condition may be assessed via entropy generation minimization (EGM). Many systems have been studied with this technique which utilizes the second law of thermodynamics to enable a more refined appraisal of heat transfer and mitigation of losses. In applying EGM, the entropy generation rate and Bejan number are usually computed. EGM has been employed in many complex multi-physical flows in recent years including combustion [36], thermally-stratified porous media flows [37], unsteady variable viscosity polymeric coating flows [38], periodic magnetohydrodynamic convection flows [39], Von Karman swirling flows [40], free convection in wavy enclosures for solar energy [41] and hydromagnetic micropolar channel flows [42]. In nanofluid mechanics, EGM has been applied in optimizing nanoscale slip flows with transpiration [43], stretching sheet nanofluid flows [44] and transient stagnation point flows with simultaneous electrical and magnetic field effects. These studies have all shown that deeper insight into thermo-physics is provided with entropy generation analysis which is beneficial for thermal designers.

The objective of the present paper is to investigate the entropy generation in natural convection thin film boundary layer flow of an Ostwald-de Waele power-law nanofluid along an inclined plate. The viscous incompressible nanofluid model developed by Buongiorno [7] (which includes the effects of Brownian motion and thermophoresis), is revised so that the nanofluid particle fraction (concentration) on the boundary is passively rather than actively controlled. Instead of deploying the commonly used conditions of constant surface temperature (isothermal) or constant heat flux (iso-flux), a *convective boundary condition* is employed. The model developed herein is therefore more comprehensive and more realistic for actual nano-coating process simulation. To the best of the authors' knowledge the present work constitutes a novel contribution to the

literature. The local non-similar equations are derived and solved numerically with a shooting method and the symbolic software MATLAB bvp4c solver. Graphs and tables are presented to illustrate the impact of key parameters on important hydrodynamic, thermal and nano-particle concentration features of the flow. The accompanying discussion provides extensive physical interpretations of the results.

2. Mathematical Model

Consider the gravity-driven accelerating laminar two-dimensional flow of a non-Newtonian power-law nanoliquid film flowing down an inclined plane surface, as shown schematically in **Fig.1**. The *x*- axis is taken along the wall in the direction of the flow and the *y* – axis taken normal to the *x*- axis. The incompressible and inelastic fluid is assumed to obey the Ostwald-de-Waele power law model and the action of viscous stresses is confined to the developing momentum boundary layer adjacent to the solid surface. The non-Newtonian nanofluid model incorporates the effects of Brownian motion and thermophoresis, following the Buongiorno approach. It is also assumed that all the fluid properties are constant except that of the influence of the density variation with temperature and the nanoparticles volume faction in the body force term (Boussinesq's approximation). The governing conservation equations for mass, momentum, energy and nanoparticle volume fraction (species i.e. concentration) within the viscous boundary layer are:

$$\frac{\partial u}{\partial x}+\frac{\partial v}{\partial y}=0 \tag{1}$$

$$u\frac{\partial u}{\partial x}+v\frac{\partial u}{\partial y}=g\cos\alpha+n\frac{\mu}{\rho}\left(\frac{\partial u}{\partial y}\right)^{n-1}\frac{\partial^2 u}{\partial y^2} \tag{2}$$

$$u\frac{\partial T}{\partial x}+v\frac{\partial T}{\partial y}=\alpha\frac{\partial^2 T}{\partial y^2}+\tau\left[D_B\frac{\partial C}{\partial y}\frac{\partial T}{\partial y}+\frac{D_T}{T_\infty}\left(\frac{\partial T}{\partial y}\right)^2\right] \tag{3}$$

$$u\frac{\partial C}{\partial x}+v\frac{\partial C}{\partial y}=D_B\frac{\partial^2 C}{\partial y^2}+\frac{D_T}{T_\infty}\frac{\partial^2 T}{\partial y^2} \tag{4}$$

Here $\alpha=\dfrac{k}{(\rho C)_f}$, $\tau=\dfrac{(\rho C)_p}{(\rho C)_f}$, g is the acceleration due to gravity, ρ is the fluid density, κ is the thermal conductivity, μ is the viscosity of the nanofluid, T and C are the temperature and nano-particle concentration respectively, ρ_f is the density of the base fluid and ρ_P is the density of the nanoparticles. $D_B$and D_T are the Brownian diffusion coefficient and the thermophoresis diffusion coefficient, respectively, $(\rho C)_f$ and $(\rho C)_P$ are the heat capacity of the base fluid and

the effective heat capacity of the nanoparticle material (e.g. Titanium dioxide metallic nano-particles), respectively. α is the thermal diffusivity and n is the power law index.

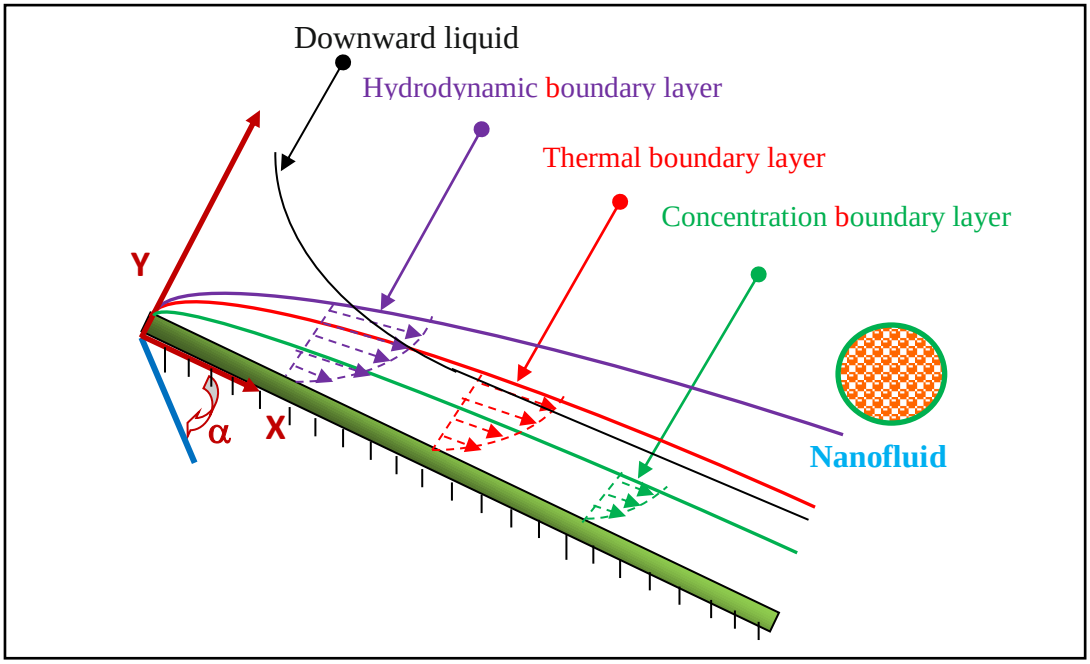

Figure 1: Physical model and coordinate system

The deviation of n from unity indicates the degree of deviation from Newtonian rheology and the particular case n = 1 represents a Newtonian fluid with dynamic coefficient of viscosity K. The boundary conditions appropriate for the regime corresponding to Eqns. (1) - (4) are:

$$u = v = 0, \quad -k\frac{\partial T}{\partial y} = h_f(x)\left(T_f - T\right), \quad D_B\frac{\partial C}{\partial y} + \frac{D_T}{T_\infty}\frac{\partial T}{\partial y} = 0 \qquad at\ y = 0$$

$$u \to u_{x,\infty}, \quad \text{as } y \to \delta_l \qquad (5)$$

$$T \to T_\infty, \quad \text{as } y \to \delta_t;\ C \to C_\infty \quad \text{as } y \to \delta_n$$

Here, $u_{x,\infty} = \sqrt{2xg\cos\alpha}$. The above equations (1) to (5) can be further non-dimensionalized using new variables:

$$\xi = \frac{x}{x_0}, \qquad \eta = \frac{y}{x}\mathrm{Re}_x^{\frac{1}{n+1}}, \qquad U = \frac{u}{\sqrt{2gx\cos\alpha}}, \qquad V = \frac{v}{\sqrt{2gx\cos\alpha}}\mathrm{Re}_x^{\frac{1}{n+1}}$$

$$\theta(\xi,\eta) = \frac{T - T_\infty}{T_f - T_\infty}, \quad \phi = \frac{C - C_\infty}{C_w - C_\infty}, \quad \mathrm{Re}_x = \frac{x^n u_{x,\infty}^{2-n}\rho}{\kappa} \qquad (6)$$

Substituting Eqn. (6) into Eqns. (1) - (5) and after some algebraic manipulation we arrive at the following transformed equations:

$$\frac{n}{n+1}\eta\frac{\partial U}{\partial \eta} - U - 2\frac{\partial V}{\partial \eta} = 0 \qquad (7)$$

$$2n\left(\frac{\partial U}{\partial \eta}\right)^{n-1}\frac{\partial^2 U}{\partial \eta^2}+\frac{n}{n+1}\eta U\frac{\partial U}{\partial \eta}-2V\frac{\partial U}{\partial \eta}-U^2+1=0 \qquad (8)$$

$$\frac{1}{\mathrm{Pr}_x}\frac{\partial^2 \theta}{\partial \eta^2}+\frac{n}{2(n+1)}\eta U\frac{\partial \theta}{\partial \eta}+Nb_x\frac{\partial \phi}{\partial \eta}\frac{\partial \theta}{\partial \eta}-V\frac{\partial \theta}{\partial \eta}+Nt_x\left(\frac{\partial \theta}{\partial \eta}\right)^2=\xi U\frac{\partial \theta}{\partial \xi} \qquad (9)$$

$$\frac{1}{Le_x}\frac{\partial^2 \phi}{\partial \eta^2}+\frac{n}{2(n+1)}\eta U\frac{\partial \phi}{\partial \eta}-V\frac{\partial \phi}{\partial \eta}+\frac{1}{Le_x}\frac{Nt_x}{Nb_x}\left(\frac{\partial^2 \theta}{\partial \eta^2}\right)=\xi U\frac{\partial \phi}{\partial \xi} \qquad (10)$$

The transformed boundary conditions emerge as:

$$U=0, \qquad V=0 \quad \frac{\partial \theta}{\partial \eta}=-\gamma(1-\theta),\ Nb_x\frac{\partial \phi}{\partial \eta}+Nt_x\frac{\partial \theta}{\partial \eta}=0 \qquad \text{at} \quad \eta=0 \qquad (11)$$

$$U\to 1, \qquad \theta\to 0, \qquad \phi\to 0 \ \text{as} \qquad \eta\to\infty \qquad (12)$$

where $\mathrm{Pr}_x=\frac{x u_{x,\infty}}{\alpha}\mathrm{Re}_x^{\frac{-2}{n+1}}$ is the local Prandtl number, $Le_x=\frac{x u_{x,\infty}\,\mathrm{Re}_x^{\frac{-2}{n+1}}}{D_B}$ is the local Lewis number, $Nb_x=\frac{\tau D_B(C_w-C_\infty)}{x u_{x,\infty}\,\mathrm{Re}_x^{\frac{-2}{n+1}}}$ is the local Brownian motion parameter, $Nt_x=\frac{\tau D_T(T_f-T_\infty)}{T_\infty x u_{x,\infty}\,\mathrm{Re}_x^{\frac{-2}{n+1}}}$ is the local thermophoresis parameter, $\gamma=\frac{h_f(x)\,x}{k\,\mathrm{Re}_x^{\frac{1}{n+1}}}$ is the thermal convective parameter, Re_x is local Reynolds number and $h_f(x)\alpha x^{-n/2(n+1)}$. For $n=1$, $h_f(x)$ is proportional to $x^{-1/4}$. We note that $n>1$ corresponds to dilatant nanofluids and $n<1$ to pseudo-plastic nanofluids. It is also noteworthy that the momentum boundary layer problem defined by the ordinary differential equations (7) and (8) subject to the relevant boundary conditions (11)-(12) is decoupled from the thermal and nanoparticle boundary layer equations. Although the hydro-dynamical problem admits similarity solutions, the accompanying thermal and nanoparticle volume fraction problem does not, since the governing equations (9) and (10) for the temperature and nanoparticle volume fraction field exhibits explicit dependencies on both ξ and η. It is therefore evident that this problem is a *non-similarity boundary layer problem* and needs to be solved by an appropriate numerical technique. In this regard we have employed the local non-similarity solution method.

3. Entropy Generation Analysis

In nanofluid flows, improvement of the heat transfer properties induces a reduction in entropy generation. However, a convection process involving a liquid film flow of nanofluids is inherently irreversible. The non-equilibrium conditions due to the exchange of energy and momentum, within the nanofluid and at the solid boundary (plate surface), cause continuous entropy generation. One

part of this entropy production results from heat transfer due to finite temperature gradients, while another part arises due to the fluid friction, nanoparticle concentration and complex interaction between the base fluid and the nanoparticles. According to Bejan [35] and later Woods [46], the *local volumetric rate of entropy generation* is given by:

$$S_g''' = \frac{k}{T_\infty^2}\left[\left(\frac{\partial T}{\partial x}\right)^2 + \left(\frac{\partial T}{\partial y}\right)^2\right] + \frac{\mu}{T_\infty}\left(\frac{\partial u}{\partial y}\right)^{n+1} + \frac{D_B}{C_\infty}\left[\left(\frac{\partial C}{\partial x}\right)^2 + \left(\frac{\partial C}{\partial y}\right)^2\right] + \frac{D_B}{T_\infty}\left[\frac{\partial C}{\partial x}\frac{\partial T}{\partial x} + \frac{\partial C}{\partial y}\frac{\partial T}{\partial y}\right] \quad (13)$$

The first term in Eq. (13) is the *irreversibility due to heat transfer*; the second term is the *entropy generation due to viscous dissipation*, while the third and the fourth terms are the *local entropy generation due to mass transfer of the nanoparticles and their complex interaction with the base fluid*. By using the boundary-layer approximation, the above equation contracts to:

$$S_g''' = \frac{k}{T_\infty^2}\left(\frac{\partial T}{\partial y}\right)^2 + \frac{\mu}{T_\infty}\left(\frac{\partial u}{\partial y}\right)^{n+1} + \frac{D_B}{C_\infty}\left(\frac{\partial C}{\partial y}\right)^2 + \frac{D_B}{T_\infty}\frac{\partial C}{\partial y}\frac{\partial T}{\partial y} \quad (14)$$

The dimensionless entropy generation number may be defined by the following relationship:

$$N_s = S_g'''\left(\delta^2 T_\infty^2 / k\left(T_f - T_\infty\right)\right) \quad (15)$$

Using non-dimensional variables, we express the entropy generation number in dimensionless form as:

$$N_s = \left(\theta'\right)^2 + \frac{Br_x}{\Omega}\left(U'\right)^{n+1} + \lambda\left(\frac{\varsigma}{\Omega}\right)^2\left(\phi'\right)^2 + \lambda\left(\frac{\varsigma}{\Omega}\right)\theta'\phi' \quad (16)$$

Here the dimensionless parameters $Br_x = \dfrac{\mu\, u_{x,\infty}^{n+1}\left(x\,\mathrm{Re}_x^{-1/n+1}\right)^{1-n}}{k\left(T_w - T_\infty\right)}$, $\Omega = \dfrac{\left(T_w - T_\infty\right)}{T_\infty}$, $\varsigma = \dfrac{\left(C_w - C_\infty\right)}{C_\infty}$, $\lambda = \dfrac{D_B\, C_\infty}{k}$ denote the local Brinkman number, temperature ratio, nano-particle concentration ratio and diffusivity ratio, respectively.

Local Skin-friction coefficient:

The gradient of the dimensionless velocity, $U(\eta)$ at the wall $\eta = 0$ is the single most important characteristic of the solution. This is due to the fact that local skin-friction coefficient $C_{x,f}$ is a

dimensionless measure of the shear stress $\tau = K\left(\frac{\partial U}{\partial y}\right)^n$ at the wall, i.e.

$$C_{x,f} \equiv \frac{\tau_w}{\frac{1}{2}\rho u_{x,\infty^2}} = \frac{K\left[\left(\frac{\partial U}{\partial y}\right)_{y=0}\right]}{\frac{1}{2}\rho u_{x,\infty^2}} \tag{17}$$

With the present dimensionless variables, the local skin-friction coefficient $C_{x,f}$ is expressed as

$$C_{x,f} \equiv \frac{\tau_w}{\frac{1}{2}\rho u_{x,\infty^2}} = 2(\mathrm{Re}_x)^{\frac{1}{1+n}}\left[\left(\frac{dU}{d\eta}\right)_{\eta=0}\right]^n \tag{18}$$

Heat and Mass Transfer Rates:

The heat transfer rate between the solid wall which is maintained at temperature T_w and liquid film is of particular significance in industrial coating applications [47, 48]. The local heat transfer rate $q_x = -k\left.\frac{\partial T}{\partial y}\right|_{y=0}$, which is governed by Fourier's law, is conveniently expressed with a local heat transfer coefficient, a_x.

$$a_x = \frac{q_x}{T_w - T_\infty} = -kx^{-1}\,\mathrm{Re}_x^{\frac{1}{n+1}}\,\theta'_{\eta=0} \tag{19}$$

Or, alternatively as the local Nusselt number:

$$Nu_x = \frac{a_x x}{k} = -\mathrm{Re}_x^{\frac{1}{n+1}}\,\theta'_{\eta=0} \tag{20}$$

Similarly, nanoparticle volume fraction transfer rate at the solid surface can be expressed as a local Sherwood number defined as:

$$Sh_x = -\mathrm{Re}_x^{\frac{1}{n+1}}\,\phi'_{\eta=0} \tag{21}$$

Here we observed that $Nu_x \propto x^{\frac{n+2}{2(n+1)}}$ and $Sh_x \propto x^{\frac{n+2}{2(n+1)}}$. It should be noted that for an analysis of Sherwood numbers, it is possible to study only Nusselt numbers since at the wall we have $\frac{\partial \phi}{\partial \eta} = -\frac{Nt_x}{Nb_x}\frac{\partial \theta}{\partial \eta}$ taking into account boundary condition for ϕ. Therefore, for further analysis it follows that $Sh_x = -\frac{Nt_x}{Nb_x}Nu_x$.

4. Results and Discussion

The nonlinear, coupled dimensionless partial differential equations (7) - (10) subject to the boundary conditions (11)-(12) are solved numerically by using local non-similarity method. This

technique was introduced by Minkowycz *et al.* [49]. Firstly, the partial differential equations (7) - (10) are transformed into ordinary differential equations using the local non-similarity boundary layer approach. Next the equations with resultant boundary conditions are solved numerically in conjunction with shooting method and MATLAB **bvp4c** solver. For the sake of brevity, the numerical method is not described explicitly here- further details are available in Vasu and Ray [23] and Bég *et al*. [50, 51]. For selected thermo-physical parameters, we have discussed the distributions velocity, temperature, nanoparticle concentration fields and entropy generation. The boundary layer problem has been solved numerically for different values of the power-law index *n*, and in the computations the following default values of parameters are prescribed (unless otherwise stated): *n = 0.5 (pseudo-plastic i.e. shear thinning nanofluid for which* viscosity decreases under shear strain), *Prx = 10 (water-based or low-density polymeric nanofluids for which momentum diffusivity substantially exceeds thermal diffusivity), Nbx =0.5 (strong Brownian motion and smaller spherical nano-particles), Ntx = 0.5 (weak thermophoretic body force), Lbx = 0.5 (nano-particle species diffusivity is double the thermal diffusivity), γ = 0.5 (significant thermal convection contribution at the wall)*. The resulting non-similarity solutions for the dimensionless velocity, temperature and nanofluid volume fraction are displayed in **Figs. (2) – (10).**

In order to assess the accuracy of the numerical solution, tabulated results of $dU/d\eta$ *and* $d\theta/d\eta$ for different values of η when *n = 0.5, Prx = 10, Nbx = Ntx = Lbx = 0* have been produced. A comparison of the present results with the local non-similarity solution as reported by Shang and Anderson [4] (achieved by neglecting nanoscale, convective boundary condition and mass transfer effects in the present model) is shown in **Table 1**. We may observe that the present results are in excellent agreement with literature data.

Table 1: *Comparison of* $dU/d\eta$ *and* $d\theta/d\eta$ (velocity gradient and temperature gradient) for different values of η when *n = 0.5, Prx = 10, Nbx = Ntx = Lbx = 0*.

η	**Shang and Anderson [4]**		**Present MATLAB Results**	
	$dU/d\eta$	$d\theta/d\eta$	$dU/d\eta$	$d\theta/d\eta$
0	1.104406	-1.139345	1.104409	-1.139346
0.1	1.001948	-1.137857	1.001952	-1.137859
0.2	0.905206	-1.127787	0.905208	-1.127789
0.3	0.814695	-1.101675	0.814696	-1.101677
0.4	0.730722	-1.054052	0.730727	-1.054055
0.5	0.653416	-0.982272	0.653418	-0.982275
0.6	0.582748	-0.887155	0.582750	-0.887158
0.7	0.518561	-0.773095	0.518564	-0.773099
1.0	0.361926	-0.397539	0.361929	-0.397541

1.6	0.17416	-0.026229	0.174163	-0.026232
2.0	0.108331	-0.001286	0.108332	-0.001286
2.5	0.061694	-0.000007	0.061695	-0.000007

The numerical results of the dimensionless velocity, temperature and nanoparticle concentration gradient at the wall are given in **Table 2** from which it is observed that the velocity gradient gradually decreases with increasing *n*. In other words, as we progress from shear-thinning (pseudoplastic, $n<1$) to dilatant (shear-thickening, $n>1$) nanofluid behaviour, there is a strong deceleration in the flow and indeed this has also been documented in experimental studies including Chen *et al.* [22]. This may be attributable to the greater agglomeration effect in nano-particles in the vicinity of the wall with dilatant (higher viscosity) behaviour which is less prevalent in lower viscosity pseudo-plastic behaviour [20]. However it is also worth noting that the local Reynolds number, Re_x, varies as $\propto x^{\frac{(n+2)}{2}}$, the streamwise variation of C_f becomes $C_f \propto x^{-\frac{n+2}{2(n+1)}}$ i.e., the *skin-friction coefficient* decreases in the streamwise direction, irrespective of the value of the power-law index.

Table 2: Dimensionless velocity, temperature and nanoparticle concentration gradients at the wall for various power-law index n.

n	$\left.\frac{dU}{d\eta}\right\|_{\eta=0}$	$\left.\frac{d\theta}{d\eta}\right\|_{\eta=0}$	$\left.\frac{d\phi}{d\eta}\right\|_{\eta=0}$
0.2	1.69549794	-0.22753241	0.22753241
0.3	1.27998541	-0.22735804	0.22735804
0.5	0.98375892	-0.22980187	0.22980187
0.7	0.88088775	-0.23330587	0.23330587
1.0	0.82689869	-0.23859899	0.23859899
1.2	0.81571131	-0.24179620	0.24179620
1.5	0.81329634	-0.24598178	0.24598178
2	0.82340898	-0.25004071	0.25004071

Also, inspection of the results presented in **Table 2** indicates that the opposite behaviour is noticed for temperature gradients associated with the Nusselt number which are seen to *increase in magnitude* with increasing power-law rheological index. This implies that dilatant nanofluids achieve enhanced heat transfer rates at the wall and this has also been corroborated by experiments reported in Raghulnath *et al.* [52] and Akhavan-Behabadi *et al.* [53] for metallic nanofluids. This is surmised to be a result of larger concentrations of nano-particles associated with smaller sized-

nanoparticles (higher Brownian motion number). Furthermore, the agglomeration phenomenon in the vicinity of the wall results in a significant clustering of nano-particles around the solid surface in the boundary layer. This increases the Sherwood number ($Sh_x = -\frac{Nt}{Nb} Nu_x$ and from this relation we have $\frac{\partial \phi}{\partial \eta} = -\frac{Nt}{Nb}\frac{\partial \theta}{\partial \eta}$) at the plate i.e. leads to an *elevation in nano-particle mass transfer rate to the plate.*

Table 3: Gradient functions, $dU/d\eta, d\theta/d\eta \, and \, d\phi/d\eta$ for different values of η when *n = 0.5, Prx = 1, Nbx = Ntx = Lbx = 0.5,* γ *= 0.5.*

η	$dU/d\eta$	$d\theta/d\eta$	$d\phi/d\eta$
0	0.82341	-0.25004	0.25004
0.1	0.79241	-0.25000	0.24998
0.2	0.76038	-0.24976	0.24967
0.3	0.72739	-0.24917	0.24885
0.4	0.69355	-0.24806	0.24733
0.5	0.65895	-0.24631	0.24489
0.7	0.58790	-0.24040	0.23666
0.85	0.53467	-0.23371	0.22731
1	0.48095	-0.22486	0.21496
1.25	0.38834	-0.20455	0.18673
1.5	0.30056	-0.17938	0.15226
1.7	0.23306	-0.15616	0.12118
2	0.14197	-0.119366	0.07394

Table 3 shows the rates of physical quantities for different η for the present study when *n = 0.5, Prx = 1, Nbx = Ntx = Lbx = 0.5,* γ *= 0.5.* It is apparent that skin friction coefficients are decreased as increasing the distance from the inclined wall normal to the flow direction (i.e. into the boundary layer region) whereas the opposite behaviour is noticed for temperature gradients associated with the Nusselt number. However as with the skin friction, there is a depletion in the nano-particle concentration gradient with progress into the boundary layer transverse to the wall and this verifies the earlier results described relating to greater Sherwood numbers always being computed at the wall, associated with the agglomeration of nano-particles (although the effect is somewhat weaker for pseudo-plastic nanofluids compared with dilatant nanofluids, as noted in [22, 52, 53]).

In **Figs. 2-10** distributions for velocity, temperature, nano-particle concentration and entropy generation rate have been computed with transverse coordinate (η). Here, f(η_δ) is the normalized stream function and the dimensionless boundary layer thickness η_δ is defined as the value of η for which the normalized velocity in Fig. 2 becomes equal to 0.99. Fig 2 indicates that the velocity behaviour of shear thinning and shear thickening nanofluids deviates substantially. It is evident

that the velocity of shear thinning fluid ($n < 1$) is higher than shear thickening fluids ($n > 1$). This is due to the elevation in shear rate which leads to decrease in viscosity of shear thinning fluids whereas it manifests in an increase in viscosity of shear thickening fluids. The momentum diffusion rate is therefore faster for pseudo-plastic nanofluids and slower for dilatant nanofluids. The former are accelerated and the latter are decelerated. For dilute nanofluids, as considered here, it is assumed that nano-particles are homogenously distributed in the boundary layer, although inevitably there is a disproportionate agglomeration at the solid surface. Nano-particles tend to benefit the momentum diffusion rate (by viscosity modification) therefore in particular near the wall. However, with further distance from the wall the lower percentage of nano-particles results in a reverse in the acceleration experienced closer to the wall, as noted by Chen *et al*. [22]. In the proximity of the edge of the boundary layer however dilatant fluids therefore achieve better flow acceleration than pseudo-plastic nanofluids. Studart *et al*. [26] have shown that there is in fact a transition region for the influence of power-law rheology on metallic nanofluid velocity distributions which is controlled by the distance from the wall. This is exactly the trend computed in fig. 2. It may be judicious also in future studies to consider the impact of *turbulence* in this transitional region which is neglected in the present laminar simulations. Asymptotically smooth profiles have been computed for all values of the rheological index parameter confirming that a sufficiently large infinity boundary condition has been prescribed in the MATLAB program. Fig 2 also shows that the temperature decreases as n increases i.e. the thermal boundary layer become thinner while power law index increased. This trend is sustained throughout the boundary layer regime from the wall to the freestream, unlike the velocity profiles which, as elaborated earlier, experience different modifications due to a combination of nanofluid rheology and distance from the wall. The increase in viscosity is assistive to thermal diffusion but inhibitive to momentum diffusion. This heats the nanofluid with increasing shear-thickening properties. In conjunction with the supplementary thermal conduction provides by small solid nano-particles, there is substantial heat transfer enhancement to the nanofluid. Furthermore nano-particles offer the advantage that they do not cause problems typically associated with larger (micro/milli-sized particles) including sedimentation effects or clogging which causes pressure drop and erosion in addition to poor stability in suspensions. Figure 2 also shows the nanoparticle volume fraction (concentration) behaviour for different power-law index values. It is evident that nanofluid volume fraction strongly decreases with power-law rheological index, n. Nano-particle diffusion is therefore assisted for pseudo-plastic nanofluids and opposed with dilatant nanofluids since the momentum diffusion is greater in the former. The nanofluid volume fraction is rapidly raised near the inclined plate and peaks close thereafter, irrespective of the power-law index. Convergent solutions are also

obtained once again in the free stream indicating that an adequately large infinity boundary condition has been used in the computations. Overall, therefore the rheological effect is easily simulated with the power-law model for nanofluids using a Buongiorno double diffusive framework. This model is simple and when combined with Buongiorno's nanoscale model circumvents the need to examine explicitly the nano-particle volume fraction in simulations. There are other models available e.g. Tiwari-Das model, which many researchers (e.g. [29]) have explored. However, they do not permit the inclusion of Brownian motion or thermophoresis effects which have been shown experimentally to contribute significantly to nanofluids. Both experimentally and theoretically power-law models provide a quantifiable framework for nanofluid rheology, which other more elegant non-Newtonian models currently do not offer (viscoelastic, memory, micropolar non-Newtonian fluids etc).

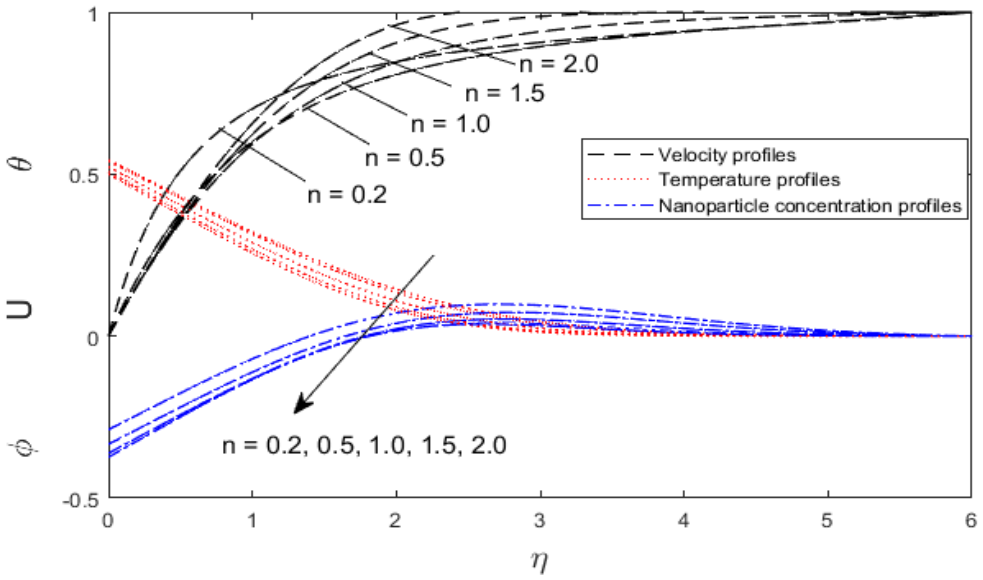

Figure 2 Effect of n on velocity distribution, temperature distribution and nanofluid volume fraction distribution

Figures 3 depicts the effect of the convective parameter (**γ**) on velocity (U), temperature (θ) and nanofluid volume fraction (**ϕ**). Velocity field is generally invariant to convective parameter and this has also been reported in numerous other studies e.g. Uddin *et al*. [34]. We may observe that for larger values of **γ**, temperature, θ is significantly larger and this induces a thickening effect on the thermal boundary-layer. The convective parameter (**γ**) is the ratio of the hot fluid side convection resistance to the cold fluid side convection resistance on the surface of the inclined plate surface. γ is directly proportional to the heat transfer coefficient h_f, for fixed cold fluid properties and is associated with the hot fluid. The thermal resistance on the hot surface side is inversely proportional to h_f. Therefore, convection resistance decreases on the hot fluid side when

γ increases and consequently, the surface temperature increases. It is also seen that for large values of **γ** i.e. $\gamma \to \infty$ the temperature profile attains its maximum value of 1. Therefore, the convective boundary condition in this limit approaches the constant surface temperature ("isothermal") case. Higher values of $\boldsymbol{\gamma}$ imply stronger convective heating at the plate, which increases the temperature gradient at the plate. However, an increase in $\boldsymbol{\gamma}$ leads to a reverse effect for the volume fraction in the boundary layer, in the proximity of the wall (solid surface) although further from the plate where nano-particle concentrations are customarily higher there is an enhancement in nano-particle volume fraction with higher convective parameter. Nano-particle concentration boundary layer is therefore not homogenously modified with greater convective parameter. As mentioned earlier since the effect of the convective parameter ($\boldsymbol{\gamma}$) is not significant on velocity distribution, there is no tangible effect on momentum boundary layer thickness.

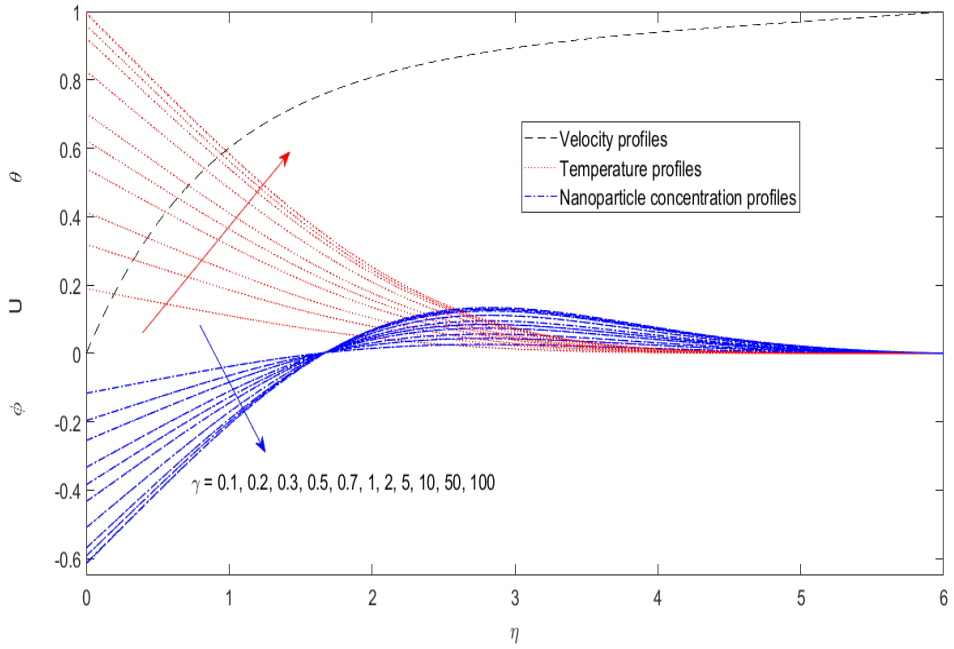

Figure 3 Effect of γ on velocity, temperature and nanofluid volume fraction distribution

Figure 4 shows that increasing Nb_x induces a strong rise in nanoparticle volume fraction for both air and water based nanofluids. With larger values of Nb_x the nano-particle concentration boundary layer thickness increases and nano-particle fractions are strongly enhanced near the solid surface. The influence of the Brownian motion parameter (Nb_x) is not significant on velocity and temperature distribution. This is logical for thin film flows since although Brownian motion of nanoparticles can enhance thermal conductivity, the regime is very thin and discourages effective heating. Larger thicker films generally achieve thermal enhancement more effectively since nanoparticles micro-convection (heat transfer surrounding individual nanoparticles) is more favourable.

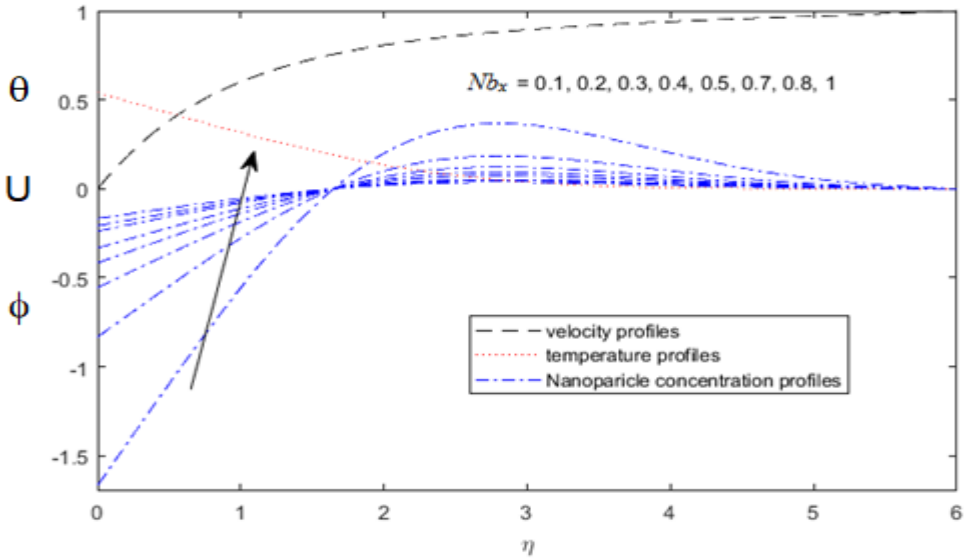

Figure 4 Effect of Brownian motion Nb_x

Figure 5 shows the nanoparticle volume fraction fields, for different values of thermophoresis parameters Nt_x. Increasing Nt_x tends to reduce the magnitude of nanoparticle concentration, so it decrease nanoparticle volume fraction concentration. Greater thermophoresis implies stronger migration of nano-particles under a temperature gradient away from the inclined surface. This decreases nano-particle concentration in the boundary layer and therefore also concentration boundary layer thickness is slightly reduced. These patterns concur with many other studies (both Newtonian and non-Newtonian) including Hayat *et al*. [27].

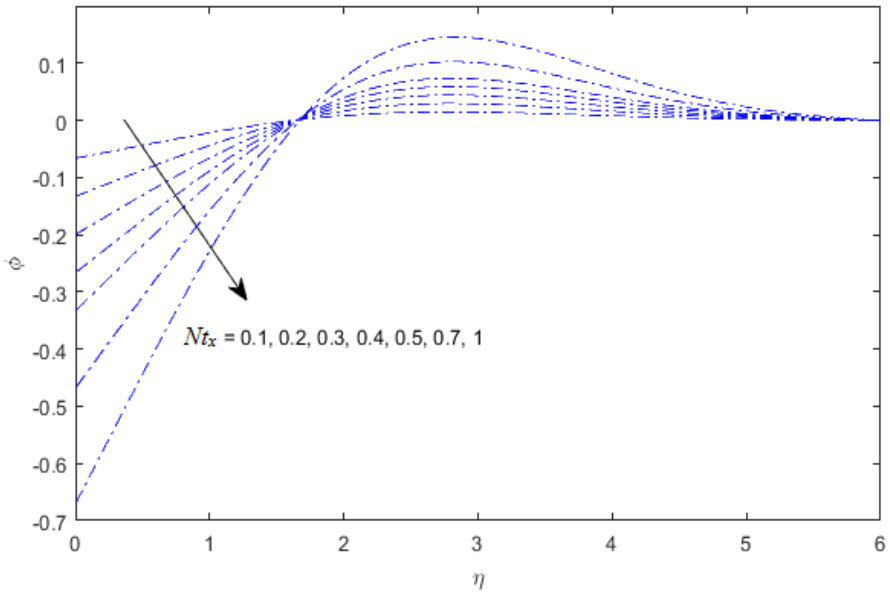

Figure 5. Effect of Nt_x on nanofluid volume fraction distribution

Figure 6 displays the effect of local Prandtl number *Prx* on temperature and nanoparticle concentration distribution for pseudo-plastic nanofluid (n = 0.5). Prandtl number is the ratio of

momentum diffusivity to thermal diffusivity in the boundary layer regime. The thickness of the thermal boundary layer decreases monotonically with increasing *Prx* from 0.2 through 0.5 to 2 for pseudo-plastic nanofluid (n = 0.5). The temperatures in the nanofluid regime will be decreased with a rise in *Prx*. Thermal boundary layer thickness will also be markedly decreased. Conversely, an increase in *Prx* raises the nanoparticle concentration boundary layer thickness. Similarly increasing Prandtl number is also found to initially boost the nanoparticle concentration values (closer to the plate surface); however, further from the surface this behaviour is reversed and an increase in local Prandtl number is observed to marginally decrease concentration values.

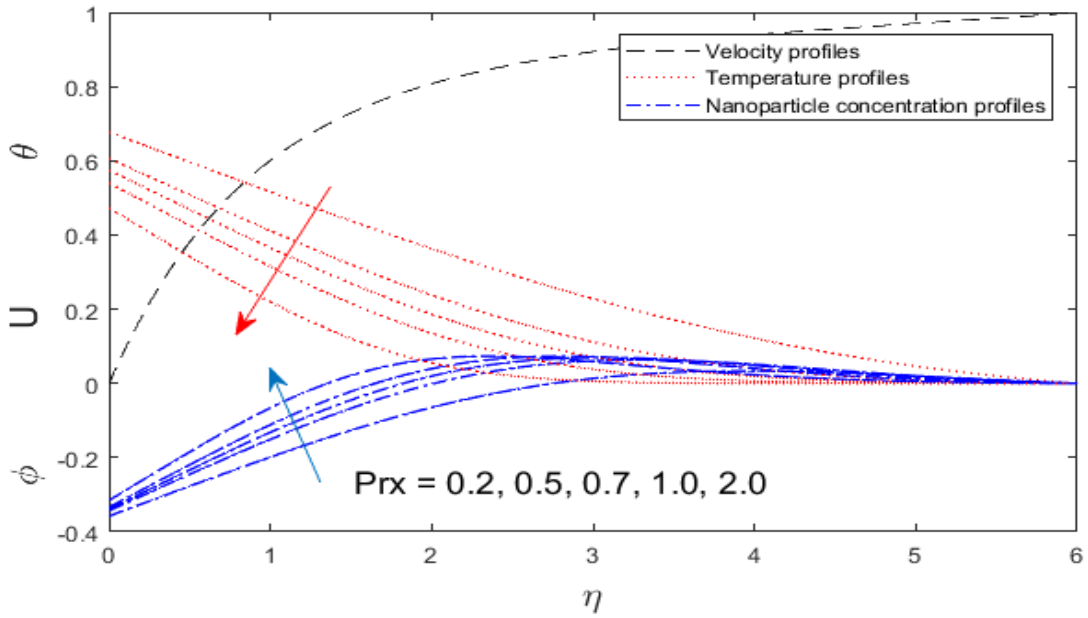

Figure 6 Effect of *Prx* on temperature distribution and nanoparticle concentration distribution

The effect of the power law index n on the magnitudes of entropy generation number is illustrated in Fig. 7. An increase of the *n* results in a reduction of entropy generation number *Ns*. A decrease in the entropy generation produced due to fluid friction occurs with increasing the value of power-law rheological index since the viscosity of the nanofluid is altered and this manifests in significant resistance to the flow. The same behaviour is observed with Brownian motion parameter (Nb_x) and thermophoresis parameter (Nt_x) on entropy generation number *Ns* from figures (8) and (9). With increasing Brownian motion effect there is an exacerbation in the ballistic collisions between nano-particles (higher *Nb* implies smaller nano-particles and greater mobility). This energizes the fluid and reduces entropy generation associated with losses. A similar observation has been made in [15, [16] and [24]. It is also worth mentioning, as noted in Chen *et al.* [22] that in pseudoplastic nanofluid high shear flows (e.g. boundary layers), Brownian motion is more prominent relative to convection whereas for lower shear flows the opposite is observed in experiments.

.

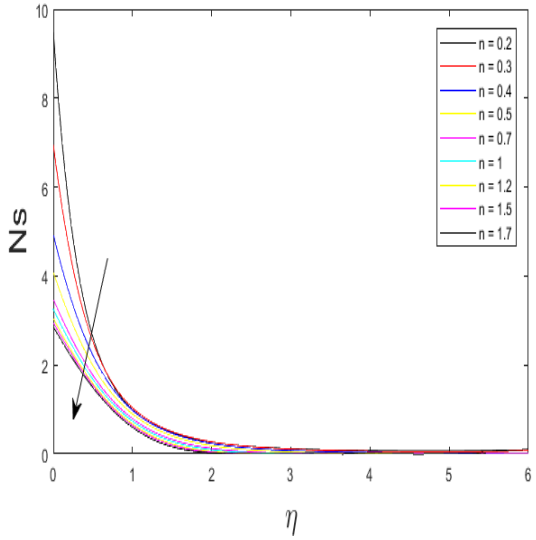

Figure 7 Effect of *n* on Entropy generation distribution

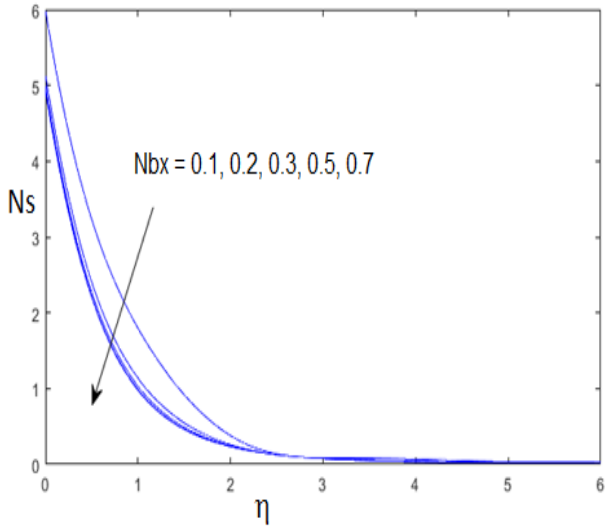

Figure 8 Effect of *Nbx* on Entropy generation distribution

Fig. 10 indicates that magnitudes of entropy generation number increase with an increase in the viscous dissipation parameter (Br_x/Ω**).** For Br_x/Ω =0 viscous heating effects are neglected. An increase in nanofluid friction results in an increase of entropy generation. In all cases entropy generation is found to be maximum at the surface. Therefore, when viscous dissipation is neglected in simulations, entropy generation rates are significantly under-predicted. For thermodynamic optimization of thin film nano-coating flows therefore it is judicious to include dissipation effects to predict more accurately the rate of entropy generation.

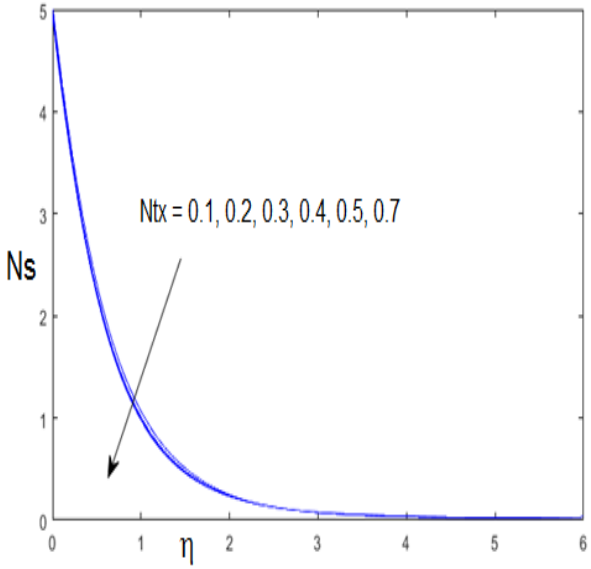

Figure 9 Effect of Ntx on Entropy generation distribution

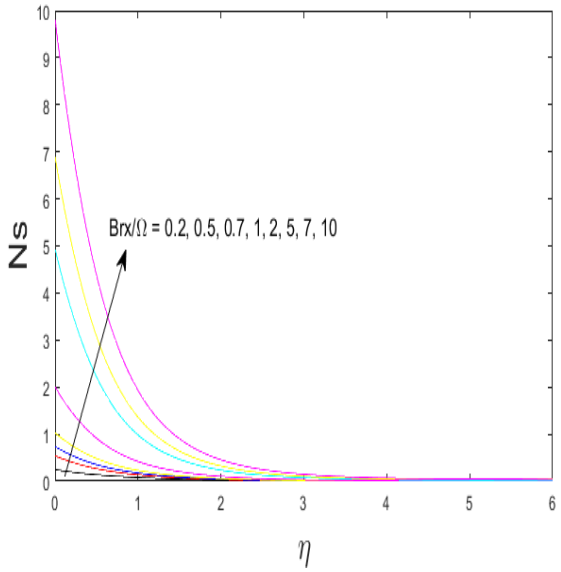

Figure 10 Effect of Br_x/Ω on Entropy generation distribution

5. Concluding Remarks

A mathematical model has been developed for non-similar heat transfer from an inclined plane surface due to an accelerating liquid film of a power-law nanofluid as a simulation of thermal nano-coating deposition processes in manufacturing. The first and second laws of thermodynamics have been employed in order to study hydrodynamics along with heat and mass transfer phenomena. Thermal and nanoparticle species boundary layer equations are derived in non-similarity form and hence a numerical solution for the emerging boundary value problem is developed using the accurate local non- similarity solution method in conjunction with shooting method. The resulting transformed problem involves several independent parameters. Accurate numerical results were obtained for various combinations of these parameters. Validation with earlier studies has been included for the case where nanoscale effects are ignored. Based on the obtained graphical and tabular results, the following conclusions can be drawn:

(i) An increase in power-law rheological index (n) produces higher entropy generation numbers (Ns).

(ii) An elevation in entropy generation is produced by increasing viscous dissipation (Brinkman number).

(iii) Entropy generation is reduced strongly with increasing Brownian motion (Nbx) but weakly decreased with increasing thermophoresis parameter (Ntx).

(iv) A significant reduction in entropy generation is induced with increasing power-law rheological parameter (n). Effectively strongly pseudoplastic nanofluids achieve higher entropy generation rates (due to lower viscosity) than dilatant nanofluids. Entropy generation in Newtonian fluids fall between these two extremes. Nanofluid rheological characteristics exert a substantial effect on entropy generation.

(v) An increase in convective parameter (γ) enhances temperature, thermal boundary layer thickness, boosts the momentum in the boundary layer and increases entropy generation (Ns) values.

(vi) With increasing local Prandtl number (Pr_x) there is an increase in thickness of the thermal boundary layer decreases monotonically for pseudo-plastic nanofluids ($n = 0.5$).

(vii) Larger values of Brownian motion (Nb_x) produce an increase in nano-particle concentration boundary layer thickness.

(viii) Increasing thermophoresis parameter (Nt_x) results in a reduction in nanoparticle concentration magnitudes.

(ix) Velocities computed for pseudo-plastic i.e. shear thinning nanofluids ($n < 1$) are higher than dilatant i.e. shear thickening nanofluids ($n > 1$) since an increase in shear rate leads to a

decrease in viscosity of shear thinning fluids whereas it elevates the viscosity of shear thickening fluids.

(x) Higher convective parameter (**γ**) manifests in stronger convective heating at the plate, which increases the temperature gradient at the plate.

The present study has revealed some interesting characteristics in entropy generation of power-law nanofluids relevant to inclined plate nano-coating systems. However, attention has been confined to *steady-state* laminar flows. Future investigations may consider *unsteady* flows and possibly turbulence with computational fluid dynamic software.

Acknowledgements

The authors wish to express their gratitude to the reviewer who highlighted important areas for improvement in this article and who has made suggestions which have served to enhance the clarity and depth of the interpretation.

References

[1] Wang C., Analytic solutions for a liquid thin film on an unsteady stretching surface, *Heat Mass Transf*, 2006, Vol. 42, P. 759–66.
[2] Andersson, H. I., and Irgens, F. Gravity-driven laminar film flow of power-law fluids along vertical walls. *Journal of Non-Newtonian Fluid Mechanics*, 1988, Vol. *27*, *No.*2, P.153-172.
[3] Gorla, R.S.R. and Nee, Y.L., Heat transfer in the thermal entrance region of a laminar non-Newtonian falling liquid film, *Int. J. Heat and Fluid Flow*, 1989, Vol.10, No.2, P.166-169.
[4] Shang D. Y., Anderson H.I., Heat transfer in gravity-driven film flow of power-law fluids, *Int J Heat Mass Transf*, 1999, Vol.42, P.2085-2099.
[5] Gorla, R.S.R., Byrd, L.W. and Pratt, D.M. Entropy minimization in micro-scale evaporating thin liquid film in capillary tubes. *Heat and Mass Transfer*, 2008, Vol.45, No.2, P.131-138.
[6] Choi S.U.S. Enhancing thermal conductivity of fluids with nanoparticles. In: Siginer, D.A, Wang, H .P. (eds.) *Development and Applications of non-Newtonian Flows*, 1995, Vol.231, P.99–105, ASME, New York,.
[7] K. R. Sharma, Process considerations for nanostructured coatings, In *Anti-Abrasive Nanocoatings, Current and Future Applications,* 2015, Pages 137-153 (2015).
[8] H.T. Phan *et al.,* Surface wettability control by nanocoating: The effects on pool boiling heat transfer and nucleation mechanism, *International Journal of Heat and Mass Transfer,* 2009, Vol. 52, P. 5459-5471.
[9] O. Anwar Bég, S. Kuharat, R. Mehmood, Rabil Tabassum and M. Babaie, Oblique radiative solar nano-polymer gel coating heat transfer and slip flow: manufacturing simulation, *ICHTFM 2018: 20th International Conference on Heat Transfer and Fluid Mechanics, Istanbul, Turkey, August 16 – 17* (2018).
[10] A.Sorrentino, *Nanocoatings and Ultra-Thin Films Technologies and Applications,* Woodhead Publishing Series in Metals and Surface Engineering, USA, 2011, P 203-234.
[11] A. Ullah, Nanofluids thin film flow of Reiner-Philippoff Fluid over an unstable stretching surface with Brownian Motion and Thermophoresis effects, *Coatings*, 2019, Vol. 9(1), P.21.

[12] Buongiorno J, Convective transport in nanofluids. *ASME J. Heat Transf*. 2006, Vol. 128, P.240-250.
[13] Tiwari RK, Das MK, Heat transfer augmentation in a two-sided lid-driven differentially heated square cavity utilizing nanofluids. *Int J Heat Mass Transfer*, 50, 2002–2018 (2007).
[14] Pak, B.C., Cho, Y.I.: Hydrodynamic and heat transfer study of dispersed fluids with submicron metallic oxide particles. *Exp. Heat Transf*. 11(2), 151–170 (1998).
[15] Kuznetsov A. V., Nield D. A., Natural convective boundary-layer flow of a nanofluid past a vertical plate, *Int. J. Therm. Sci.*, 2010, Vol.49, No.2, P.243-247.
[16] D. Tripathi, A. Sharma, O. Anwar Bég, Joule heating and buoyancy effects in electro-osmotic peristaltic transport of aqueous nanofluids through a microchannel with complex wave propagation, *Advanced Powder Technology*, 2018, Vol. 29, P. 639-653.
[17] R.M. Kasmani *et al.,* Laminar boundary layer flow of a nanofluid along a wedge in the presence of suction/injection, *Journal of Applied Mechanics and Technical Physics*, 2013, Vol. 54, P. 377–384.
[18] S. Kuharat, O. Anwar Bég, Ali Kadir and M. Babaie, Computational fluid dynamic simulation of a solar enclosure with radiative flux and different metallic nano-particles, *International Conference on Innovative Applied Energy (IAPE'19), St. Cross College, University of Oxford, United Kingdom, 14-15 March* (2019).
[19] P. Loganathan *et al.,* Transient natural convective flow of a nanofluid past a vertical plate in the presence of heat generation, *Journal of Applied Mechanics and Technical Physics*, 2015, Vol. 56, P. 433–442.
[20] A. Ahmadi *et al.,* Evaluating the effects of different parameters on rheological behavior of nanofluids: A comprehensive review, *Powder Technology*, 2018, Vol. 338, P. 342-353.
[21] A.K.Sharma *et al.,* Rheological behaviour of nanofluids: A review, *Renewable and Sustainable Energy Reviews*, 2016, Vol. 53, P.779-791.
[22] H. Chen *et al.*, Rheological behaviour of nanofluids, 2007 *New J. Phys.* Vol. 9, P. 367.
[23] Vasu B., Atul Kumar Ray, Numerical study of Carreau nanofluid flow past vertical plate with the Cattaneo–Christov heat flux model, *International Journal of Numerical Methods for Heat & Fluid Flow*, 2018, https://doi.org/10.1108/HFF-03-2018-0104
[24] I.S. Oyelakin *et al.*, Unsteady Casson nanofluid flow over a stretching sheet with thermal radiation, convective and slip boundary conditions, *Alexandria Engineering Journal*, 2016, Vol. 55, 1025-1035.
[25] R.S.R. Gorla and B.K. Gireesha. Convective heat transfer in three-dimensional boundary-layer flow of viscoelastic nanofluid, *AIAA Journal of Thermophysics and Heat Transfer,* 2016, Vol. 30, 334-341.
[26] Studart A R, Amstad E, Antoni M and Gauckler L J, Rheology of concentrated suspensions containing weakly attractive alumina nanoparticles *J. Am. Ceram. Soc.* 2006, Vol. 89, 2418-2425.
[27] T. Hayat *et al.*, Flow of a power-law nanofluid past a vertical stretching sheet with a convective boundary condition, *Journal of Applied Mechanics and Technical Physics,* 2016, Vol.57, P.173–179.
[28] Gorla, R. S. R., and Vasu, B., Unsteady convective heat transfer to a stretching surface in a non-Newtonian nanofluid. *Journal of Nanofluids*, 2016, Vol. 5, No.4, P.581-594.
[29] M. Ferdows and M.A.A Hamad, MHD flow and heat transfer of a power-law non-Newtonian nanofluid ($Cu–H_2O$) over a vertical stretching sheet, *Journal of Applied Mechanics and Technical Physics,* 2016, Vol.57, P.603-610.
[30] A. Aziz, W. Jamshed. Unsteady MHD slip flow of non-Newtonian power-law nanofluid over a moving surface with temperature-dependent thermal conductivity. *Discrete & Continuous Dynamical Systems - S*, 2018, 11 (4): 617-630. doi: 10.3934/dcdss.2018036
[31] Makinde, O. D., and Aziz, A. Boundary layer flow of a nanofluid past a stretching sheet with a convective boundary condition. *International Journal of Thermal Sciences*, 2011, Vol.*50, No.*7, P.1326-1332.

[32] Kameswaran, P.K., Vasu, B., Murthy, P.V.S.N., and Gorla, R.S.R., Mixed Convection from a Wavy Surface Embedded in a Thermally Stratified Nanofluid saturated Porous Medium with non-Linear Boussinesq Approximation, *Int Commn Heat Mass Trans*, 2016, Vol.77, P.78-86.
[33] O. Anwar Bég, S.S. Motsa, M.N. Islam and M. Lockwood, Pseudo-spectral and variational iteration simulation of exothermically-reacting Rivlin-Ericksen viscoelastic flow and heat transfer in a rocket propulsion duct, *Computational Thermal Sciences,* 2014, Vol. 6, 91-102.
[34] M.J. Uddin, O. Anwar Bég, P.K. Ghose and A.I.M. Ismael, Numerical study of non-Newtonian nanofluid transport in a porous medium with multiple convective boundary conditions and nonlinear thermal radiation effects, *Int. J. Num. Meth. Heat Fluid Flow,* 2016, Vol. 26, 1-25.
[35] A. Bejan, *Entropy Generation Through Heat and Fluid Flow, 1982,* Wiley, New York, USA.

[36] F. Bouras and F. Khaldi, Numerical analysis of entropy generation in a turbulent diffusion flame, *Journal of Applied Mechanics and Technical Physics,* 2016, Vol.57, P.20-26.
[37] Vasu, B., RamReddy, C., Murthy, P. V. S. N., and Gorla, R. S. R. Entropy generation analysis in nonlinear convection flow of thermally stratified fluid in saturated porous medium with convective boundary condition. *ASME Journal of Heat Transfer*, 2017, Vol.139, No.9, P.091701.
[38] G. J. Reddy, M. Kumar and O. Anwar Bég, Effect of temperature dependent viscosity on entropy generation in transient viscoelastic polymeric fluid flow from an isothermal vertical plate, *Physica A - Statistical Mechanics and its Applications*, 2018, Vol. 510, P. 426–445.
[39] A.S. Butt and A. Ali, Entropy generation effects in a hydromagnetic free convection flow past a vertical oscillating plate, *Journal of Applied Mechanics and Technical Physics,* 2016, Vol.57, P.27-37.
[40] M.M. Rashidi, N. Kavyani, O. Anwar Bég and R.S.R. Gorla, Transient magnetohydrodynamic film flow, heat transfer and entropy generation from a spinning disk system: DTM-Padé semi-numerical simulation, *Int. J. Energy & Technology*, 2013, Vol. 5, P. 1–14.
[41] S. Morsili and A. Sabeur-Bendehina, Entropy generation and natural convection in square cavities with wavy walls, *Journal of Applied Mechanics and Technical Physics*, 2013, Vol. 54, 913-920.
[42] J. Srinivas and O. Anwar Bég, Homotopy study of entropy generation in magnetized micropolar flow in a vertical parallel plate channel with buoyancy effect, *Heat Transfer Research, 2018, Vol. 49, 529–553.*
[43] A. Bhardwaj, N. Shukla, P. Rana, O. Anwar Bég, Lie group analysis of nanofluid slip flow with Stefan blowing effect via modified Buongiorno's model: entropy generation analysis, *Differential Equations and Dynamical Systems* (2019). https://doi.org/10.1007/s12591-019-00456-0 *(18 pages).*
[44] A. Noghrehabadi, M. R. Saffarian, R. Pourrajab and M. Ghalambaz, Entropy analysis for nanofluid flow over a stretching sheet in the presence of heat generation/absorption and partial slip, *Journal of Mechanical Science and Technology*, 27(3) (2013) 927–937.
[45] N. Shukla, Puneet Rana, O. Anwar Bég, A. Kadir and Bani Singh, Unsteady electromagnetic radiative nanofluid stagnation-point flow from a stretching sheet with chemically reactive nanoparticles, Stefan blowing effect and entropy generation, *Proc. IMechE: Part N-Journal of Nanomaterials, Nanoengineering and Nanosystems (2018). DOI: 10.1177/2397791418782030 (14 pages).*
[46] Woods L.C., *The Thermodynamics of Fluid Systems*, Oxford University Press. *New York*, 1975.
[47] Edgar, B.G. and Edward, D.C. *Coating and Drying Defects Troubleshooting Operating Problems.* A Wiley-Interscience Publication, New York, 1995.
[48] Liu, Z.-M., Jin, Y.-M. and Liu, H.-M. (2008) Progress on Formation and Prevention of Defects in Thin Film Coating. *Journal of Safety and Environment*, 2008, Vol. 8, P. 135-139.

[49] Minkowycz W. J., Sparrow E. M. and Murthy J. Y., *Handbook of Numerical Heat Transfer*, Second Edition, John Wiley & Sons, Inc, USA 2006.
[50] O. Anwar Bég, A.Y. Bakier, V.R. Prasad and S.K. Ghosh, Non-similar, laminar, steady, electrically conducting forced convection liquid metal boundary layer flow with induced magnetic field effects, *Int. J. Thermal Sciences, 2009*, Vol. 48, P. 1596-1606.
[51] O. Anwar Bég, M. Ferdows, Shamima Islam and M. Nazrul Islam, Numerical simulation of Marangoni magnetohydrodynamic bio-nanofluid convection from a non-isothermal surface with magnetic induction effects: a bio-nanomaterial manufacturing transport model, *J. Mechanics Medicine Biology*, 2014, Vol. 14, P. 1450039.1-1450039.32.
[52] D. Raghulnath *et al.*, Investigation of rheological behaviour and heat transfer performance of alumina nanofluid, *International Journal of Engineering Research & Technology (IJERT)*, 2016, Vol. 5 p. 57-63.
[53] M. A. Akhavan-Behabadi *et al***.,** Experimental investigation of thermal–rheological properties and heat transfer behavior of the heat transfer oil–copper oxide (HTO–CuO) nanofluid in smooth tubes, *Experimental Thermal and Fluid Science*, 2015., Vol. 68, P. 681-688.
[54] S. Aberoumand *et al.,* Experimental study on the rheological behavior of silver-heat transfer oil nanofluid and suggesting two empirical based correlations for thermal conductivity and viscosity of oil based nanofluids, *Applied Thermal Engineering,* 2016, Vol.101, P. 362-372.